




## Heterogenous westerly shifts linked to Atlantic meridional overturning circulation slowdowns

Congcong Gai<sup>1,2</sup>, Jie Wu<sup>3</sup>, Andrew P. Roberts <sup>2</sup>, David Heslop<sup>2</sup>, Eelco J. Rohling <sup>2,4</sup>, Zhengguo Shi<sup>3,5</sup>, Jianxing Liu<sup>6</sup>, Yi Zhong<sup>1</sup>, Yanguang Liu <sup>6</sup>✉ & Qingsong Liu<sup>1</sup>✉

The mid-latitude westerly winds are a major component of the global atmospheric circulation and a dominant factor in mid-latitude climate change. Understanding their behaviour and the controls on their variations under different climate background states is essential for assessing climate system feedback. Here we present a midlatitude North Pacific Ocean aeolian dust record from core NPO2 through the last glacial cycle, during which extreme and abrupt climatic oscillations occurred. We find low dust contents during Heinrich stadials 2, 4, 5, and 5a that we attribute using proxy-model comparison to westerly transportation path changes associated with Atlantic meridional overturning circulation (AMOC) reductions, which caused North Atlantic cooling and modified the westerly wave train pattern, particularly over the Tibetan Plateau. The finding that AMOC variations had significant impacts on the westerlies half-way around the world, through ocean-atmosphere interactions, improves understanding of large-scale westerly sensitivity to different climate states.

<sup>1</sup>Centre for Marine Magnetism (CM2), Department of Ocean Science and Engineering, Southern University of Science and Technology, Shenzhen 518055, China. <sup>2</sup>Research School of Earth Sciences, Australian National University, Canberra ACT 2601, Australia. <sup>3</sup>State Key Laboratory of Loess and Quaternary Geology, Institute of Earth Environment, Chinese Academy of Sciences, Xi'an 710061, China. <sup>4</sup>Ocean and Earth Science, University of Southampton, National Oceanography Centre, Southampton SO14 3ZH, UK. <sup>5</sup>Institute of Global Environmental Change, Xi'an Jiaotong University, Xi'an 710049, China. <sup>6</sup>Key Laboratory of Marine Geology and Metallogeny, First Institute of Oceanography, Ministry of Natural Resources (MNR), Qingdao 266061, China. ✉email: [yanguangliu@fio.org.cn](mailto:yanguangliu@fio.org.cn); [qslu@sustech.edu.cn](mailto:qslu@sustech.edu.cn)

Westerlies are the prevailing winds that blow from west to east between latitudes of 30° and 60° in both hemispheres and are a key component of global atmospheric circulation<sup>1</sup>. They play an essential role in transporting heat and moisture, and in balancing the energy distribution between low- and high-latitude regions<sup>2–5</sup>. The westerlies have shifted poleward since the 1960s in response to global warming, which caused more severe midlatitude weather events, such as extreme storms and precipitation<sup>6–8</sup>. The increasing effects of such extreme events make it necessary to understand how the westerlies responded to different climate states. The last glacial cycle (~115–11.6 ka) was characterized by extreme millennial climatic oscillations between cold and warm states<sup>9</sup>, and the prevailing paradigm attributes these millennial climatic oscillations to AMOC reorganizations<sup>10,11</sup>, associated with massive iceberg discharges during Heinrich (H) stadials<sup>9,12</sup>. This study investigates how these oscillations affected the downstream behaviour of the westerlies as far away as the North Pacific Ocean.

So far, geological studies of northern hemisphere westerly variations in the last glacial cycle have relied mainly on terrestrial and marginal sea sediments, using records such as those from the Chinese Loess<sup>13</sup>, Lake Qinghai<sup>14</sup>, Japan Sea<sup>15</sup>, and Philippine Sea<sup>16</sup>. Studies indicate that stronger westerlies usually occur in cold stadials<sup>17</sup>, and vice versa. However, how the westerly path changed during the last glacial cycle is still debated. Some studies suggest that the main westerly axis shifted southward during stadials<sup>14,15</sup> while others suggest the opposite view<sup>13</sup>. This controversy can be attributed largely to limitations of proxy evidence in the studied regions; unambiguous proxy indicators of the westerlies over Asia are difficult to obtain because they are also affected by the monsoon circulation<sup>16,18,19</sup>. In contrast, atmospheric circulation over the North Pacific Ocean (NPO) is dominated by the westerlies and past westerly behaviour can be inferred from NPO aeolian dust records directly or from palaeoceanographic records indirectly<sup>20–24</sup>. Considering the generally low sedimentation rates and the challenge of dating sediments deposited below the calcite compensation depth<sup>25</sup>, few late Quaternary sedimentary records from the NPO have been explored<sup>26,27</sup>. This hinders understanding of millennial-scale westerly behaviour and the underlying driving mechanisms during the last glacial cycle.

Core NP02 (40.48°N, 150.10°E, 5,177 m water depth) is located downwind of Asian dust source areas and adjacent to the main

westerly axis, which enables sensitive detection of westerly shifts (Fig. 1). A recent study suggested that core NP02 sediments were deposited at an average of ~11.6 cm kyr<sup>-1</sup> (ref. 28), so this core is expected to capture westerly responses to abrupt climate transitions between warm interstadials and cold stadials within the last glacial cycle. Here, we present a dust record for core NP02 over ~21–57 ka, and we assess westerly path changes that are compared with Transient Climate of the Last 21,000 Years (TraCE-21ka) simulation results to further assess possible underlying mechanisms.

## Results and discussion

**Core NP02 age model reconstruction.** An initial age model for core NP02 is presented in ref. 28. Here, we tuned the core NP02 geomagnetic relative paleointensity (RPI) record to RPI variations recorded in subarctic Pacific Ocean cores GC1 and PC7<sup>29,30</sup> (Supplementary Fig. 1a). Depth and age uncertainties for each tie-point are shown in Supplementary Table 1. Tie-points T2 and T6 are identified as the Rockall and Laschamp excursions in ref. 28 with ages of 26,525 ± 175 years and 41,100 ± 350 years ago, respectively<sup>31,32</sup>. Age uncertainties of tie-points T1, T3, T4, and T5 are estimated as the mean squared estimates of the reference chronology uncertainty. Tie-point depth intervals are represented by Gaussian functions, with uncertainties expressed as ±1σ.

The reconstructed age-depth model is shown in Supplementary Fig. 1b. For the intermediate part (18–395 cm) of core NP02, ages are estimated from the probability density functions using the age constraints listed in Supplementary Tables 1 and 2 with the MATLAB Undatable software<sup>33</sup>. For the upper (<18 cm) and lower (>395 cm) parts of core NP02, ages are obtained by extrapolation of linear regressions over the 23.5–26.5 ka and 45.8–54.6 ka intervals, respectively. Given that there are no independent age constraints for the upper (<18 cm) and lower parts, we have tested several fitting methods (Supplementary Fig. 2). Second-order polynomial fitting also works well for the upper parts, and age offsets between the linear regression and second-order polynomial fitting are less than 0.34 kyr. However, the second-order polynomial fitting gives unrealistically young ages at the 396–400 cm depth interval. Therefore, the second-order polynomial fitting is not used here. Moreover, we focus on the well-constrained parts of core NP02 (18–395 cm), so that the upper and lower parts with limited age constraints do not affect this study.

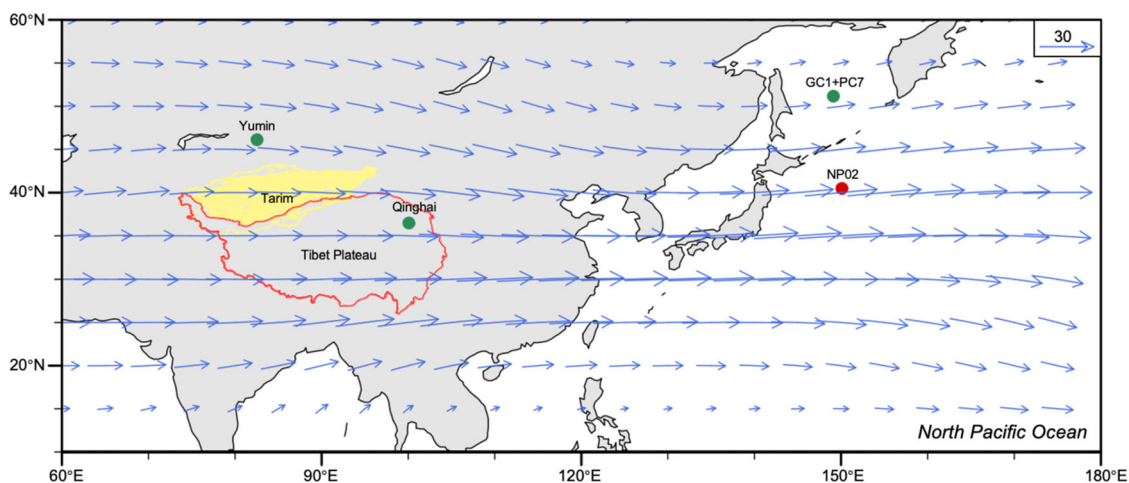


**Fig. 1 Schematic map of continental Asia and the North Pacific Ocean.** Locations of core NP02 (40.48°N, 150.10°E, red circle) and other cores mentioned in this study are indicated. The primary aeolian dust source (yellow) in central Asia is from the 1:100,000 Tarim River Basin desert distribution dataset provided by the National Tibetan Plateau Data Center (<http://data.tpdc.ac.cn>). Blue arrows indicate the wind vector (unit: m s<sup>-1</sup>) at 200 hPa in the spring between 1979 and 2020, provided by the NCEP/DOE Reanalysis II data (<https://psl.noaa.gov>).

**Dust proxy.** High-coercivity magnetic minerals – hematite and goethite – usually occur as nanoparticles in the Asian interior<sup>24,34</sup>. They have long atmospheric residence times and can be transported over long distances; therefore, they have been studied frequently as dust proxies<sup>35–39</sup>. The ‘hard’ isothermal remanent magnetization (HIRM) is used widely to evaluate the high-coercivity magnetic mineral concentration<sup>40–44</sup>. However, its interpretation can be complicated by changes in the properties of high-coercivity magnetic minerals, such as the coercivity distribution and isomorphous cation substitution<sup>45–47</sup>. The *L*-ratio enables semi-quantitative identification of coercivity variations<sup>46</sup>. Samples from the Spfa–1 and Kt-3 tephra layers in core NP02 (ref. <sup>28</sup>) have relatively high and low *L*-ratio values, respectively; some neighbouring samples also have anomalous *L*-ratio values. This is likely to result from admixed volcanic ash. After excluding tephra samples and those with anomalous values, *L*-ratio variations fall within a relatively narrow range (shaded area in Supplementary Fig. 3a), which indicates that the Al substitution degree is relatively stable (Supplementary Fig. 3b). Moreover, the magnetization acquired above 300 mT has a linear relationship with IRM carried by component 3 of IRM decomposition results<sup>28</sup> (Supplementary Fig. 4), which further supports that HIRM can be used to indicate hematite and goethite concentration variations in core NP02 sediments. Goethite is often volumetrically more abundant than hematite in sediments. For example, the goethite concentration is 2 to 3 times higher than that of hematite in loess-palaeosol sequences on the Chinese Loess Plateau<sup>48</sup>. However, its concentration is difficult to measure because <10% of its IRM is thought to be acquired at applied fields up to 3 T (ref. <sup>49,50</sup>). Therefore, HIRM provides more information about hematite content than goethite content. In core NP02, hematite variations are identified by IRM acquisition curve decomposition<sup>28</sup>. Hematite does not have an authigenic origin in the NPO<sup>38</sup> and the studied core is far from sources of riverine and ice-rafted sediment, so hematite is treated as aeolian in origin. Thus, HIRM is used here as a hematite dust concentration proxy for core NP02.

**North Pacific Ocean dust content changes and mechanisms for variability.** NPO dust is transported long distances by the westerlies in the middle and upper troposphere<sup>20,51,52</sup>, and its content variations are influenced by the location and spatial extent of dust source regions, the westerly dust transport path and efficacy, and the dust deposition process (i.e., dry deposition vs wet removal). The NPO is sedimentologically simpler than other oceans, with the Asian interior serving as the major dust source where dust storms occur mainly in spring throughout the Cenozoic<sup>22,53–55</sup>, as verified by a La-Th-Sc ternary diagram for the siliciclastic fraction in core NP02 (Supplementary Fig. 5). Extremely low kaolinite contents (<4%) throughout core NP02 indicate a lack of intense Asian interior chemical weathering<sup>56</sup> (Supplementary Fig. 6d). The smectite/(illite + chlorite) ratio does not have an obvious overall trend, with variations around 0.77 (Supplementary Fig. 6e). This lack of variability indicates that the Asian interior climate was relatively stable and arid throughout the 21–57 ka interval.

Interpretations of relationships between source regions and the climatic significance of dust remain controversial. Increased aeolian dust contents have been traditionally attributed to increased aridity. For example, increasing hematite contents at ~2.5 Ma were attributed to progressive Asian continental aridification<sup>38,57</sup>. Alternatively, it has been suggested that enhanced dust contents were caused by increased sediment availability associated with increased snow and glacial meltwater that resulted from climatic cooling<sup>39</sup>. In this interpretation,

increased aeolian dust inputs resulted from the provision of renewable sources of erodible silt that was later deflated as dust during arid climatic phases. In our results from NP02, the source area weathering regime seems to have remained constant, and neither HIRM nor the smectite/(illite + chlorite) ratio suggests any evident relationship as required in the interpretations in ref. <sup>42</sup> or ref. <sup>39</sup> (Supplementary Fig. 6e and f). Hence, we rule out dust source region variations as a primary driver of dust content changes in core NP02.

Instead, the westerlies can play an important role in controlling the observed dust content changes. Considering that westerly intensity has no obvious effect on late Quaternary dust content variations over the NPO<sup>20,58,59</sup>, we propose instead that westerly transportation pathway changes explain the dust variations in core NP02. Tropical tropospheric warming and/or polar stratospheric cooling increase the meridional temperature gradient<sup>60</sup>, which will affect the location of baroclinic instability that in turn affects westerly strength and movement<sup>60–62</sup>. For example, high-latitude North Atlantic cooling through AMOC slowdown has modulated Holocene westerlies over the western Mediterranean region<sup>63</sup>. On millennial timescales, abrupt dust content decreases in core NP02 are identified at approximately 24, 39, 48, and 54 ka, at times of H2, H4, H5, and H5a (Fig. 2d and Supplementary Data 1), as recorded in Greenland ice cores (Fig. 2a and b). The significance of these features has been tested (Supplementary Note 1) and, importantly, they all have ages that fall near multiple age tie-points or, for the oldest feature, close to a well constrained tephra age (Fig. 2d and Supplementary Fig. 1b). Studies indicate that these abrupt glacial climate changes were associated with major AMOC slowdowns<sup>64–67</sup>. The AMOC transports heat from low to high latitudes, and its slowdown reduces meridional ocean heat transport by as much as ~60% to the north of 40°N (ref. <sup>68</sup>). Moreover, modelling studies have identified that AMOC slowdown affects the midlatitude NPO through oceanic and atmospheric teleconnections<sup>69–72</sup>. Therefore, AMOC slowdowns are expected to affect the westerly path and cause dust variations in core NP02.

Similar to H2, 4, 5, and 5a, the Younger Dryas (YD) and H1 events are also considered to have been associated with major AMOC reduction<sup>73–77</sup>. Here we use outputs for the YD and H1 events from TraCE-21ka model experiments, with both full and single forcings (Supplementary Table 3), respectively, to evaluate the impacts of westerly changes on Asian dust transportation. We note that the role of orbital forcing may be underestimated as the precessional forcing is stronger in the observations (the last glacial cycle) than in the model simulations. The model-output westerly climatology forced by meltwater mimics that of the full forcings, while those of other single forcing experiments do not (Fig. 3 and Supplementary Fig. 7), which indicates a primary role of freshwater forcing in inducing circulation anomalies over Asia. Fresh glacial meltwater “hosing” into the North Atlantic Ocean at high latitudes causes a reduction of northward AMOC heat transport in the model simulations<sup>68</sup>. Based on simulated temperatures over the North Atlantic Ocean, the experiments capture rapid cooling well and are consistent with the cooling presented in other water hosing experiments<sup>78–82</sup> for the YD and H1 events. Regarding freshwater hosing in H1, the differences in westerly climatology between two 300-year periods before (19–18.7 ka) and during the peak cooling (16–15.7 ka) in freshwater-forced experiments were calculated to reflect how such a North Atlantic cooling signal affects downstream westerly circulation over Asia. The mid-latitude westerly wave train response that propagates eastward across Eurasia in the middle to upper troposphere acts to intensify atmospheric high pressures and anticyclonic circulation over the Tibetan Plateau (TP; Fig. 3a). Strengthened anticyclonic circulation drives intense southerly

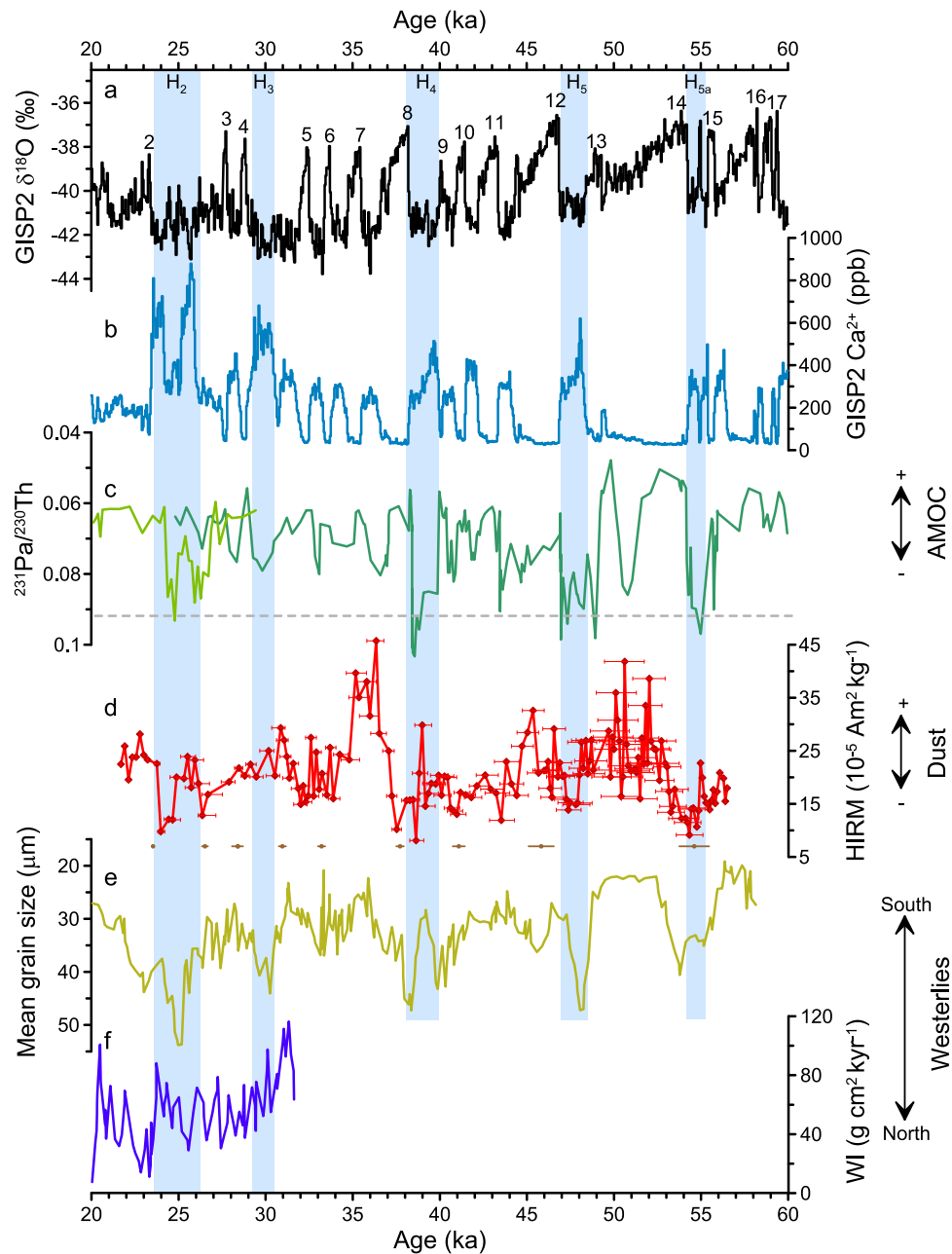


**Fig. 2** Westerly and North Atlantic climate records over the 60–20 ka interval. **a, b** GISP2  $\delta^{18}\text{O}$  and  $\text{Ca}^{2+}$  records on the GICC05modelext chronology<sup>105</sup>, respectively. **c** Sediment  $^{231}\text{Pa}/^{230}\text{Th}$ ; light and dark green curves represent records from ODP Site 1063 over the 20–30 ka interval<sup>106</sup> and core CDH19 over the 25–60 ka interval<sup>66</sup>, respectively. **d** Hard isothermal remanent magnetization (HIRM) for core NP02, plotted with error bars representing age uncertainties ( $1\sigma$ ). Brown dots with error bars below Fig. 2d denote age constraints with  $1\sigma$  uncertainties used in this study. **e** The median grain size of the Yumin loess section<sup>13</sup>. **f** Westerly climate index (WI, flux of  $>25\ \mu\text{m}$  fraction) from Lake Qinghai<sup>14</sup>. The dashed line in (c) denotes the  $^{231}\text{Pa}/^{230}\text{Th}$  production ratio of 0.093 in sea water<sup>88</sup>. Locations of Dansgaard-Oeschger interstadials (black number) and Heinrich (H) events are indicated, after ref. <sup>91</sup>.

winds to the west of the TP and intense northerly winds to its east, throughout the troposphere (Fig. 3b). The modern Asian dust transport pathway is consistent with the westerly path<sup>83</sup>; assuming that this also the case for the last glacial cycle, then these circulation changes should substantially modify dust transportation pathways in the Asian dust source region. Notably, downstream of the Asian interior, dust is more likely to be transported to the south by northerly winds, rather than eastward to the NPO. Similar changes to the westerlies are seen in the TraCE-21ka YD simulations (Supplementary Fig. 8).

The TraCE-21ka results indicate no significant meridional westerly shift over the NPO during H stadials (Fig. 3a), which is

consistent with the findings of ref. <sup>84</sup> that the main westerly axis remained at  $38\text{--}40^\circ\text{N}$  over the NPO throughout the last glacial cycle. Instead, we infer that altered westerly pathways over inland Asia (Fig. 3a) favoured dust deposition patterns on the continent during H2, H4, H5, and H5a, which—given the low HIRM values in core NP02—left less dust available for transport and deposition over the NPO (Fig. 2d). Dust contents did not decrease in core NP02 during H3 (Fig. 2d). In contrast to H2, H4, H5, and H5a, when ice-rafted debris identified in the North Atlantic Ocean was derived mostly from the Laurentide ice sheet, H3 contains ice-rafted debris derived mostly from the European ice sheet; this different source/location of iceberg input is thought to have had



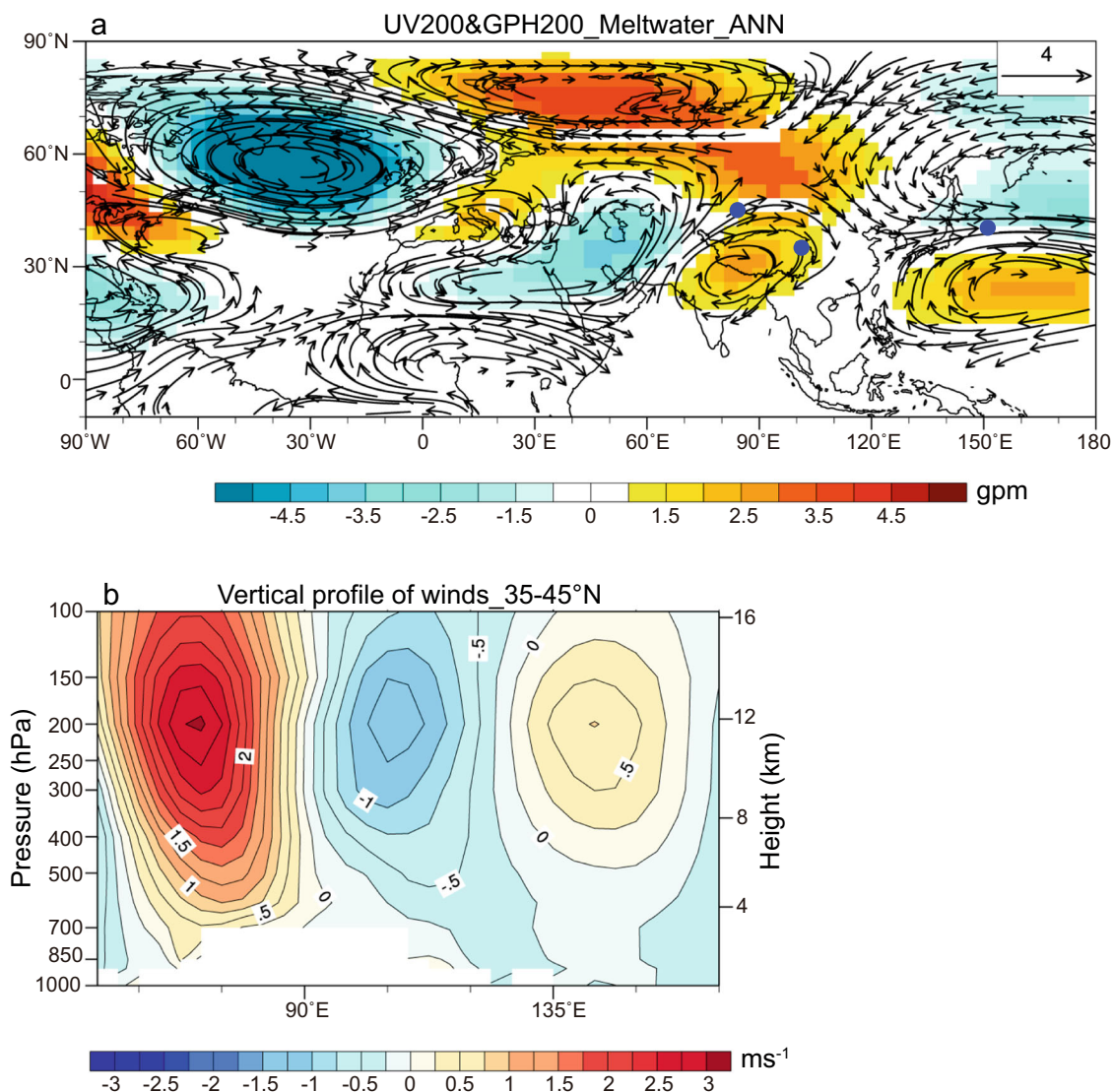


**Fig. 3** Westerly response to water-hosing in Heinrich stadial (H) 1 in the TraCE-21ka experiment. **a** 200 hPa wind vector (black arrows, in  $\text{ms}^{-1}$ ) and zonal deviations of geopotential height (filled colours, in  $\text{gpm}$ ); and **(b)** vertical profile of meridional wind velocity (filled colours, in  $\text{m s}^{-1}$ ) for 35–45°N. The differences are based on model results in the TraCE-21ka freshwater-forcing-only experiment and are denoted as those between two 300-year periods before (19–18.7 ka) and during peak cooling (16–15.7 ka) over the North Atlantic in H1, respectively. Blue dots from left to right are the locations of Yumin Loess, Lake Qinghai, and core NP02, respectively.

less impact on AMOC intensity<sup>12,85–87</sup>. Accordingly, <sup>231</sup>Pa/<sup>230</sup>Th ratios did not reach a production ratio of 0.093 during H3, which indicates less AMOC weakening<sup>88,89</sup> (Fig. 2c). AMOC during H3 is, thus, interpreted to have been relatively deep and vigorous<sup>64,67,90</sup>, compared to the other Heinrich events. We infer that a weaker northward heat transport reduction in the North Atlantic during H3 had less impact on the westerly wave train than during the other H stadials and, thus, we observe no abrupt dust content decrease in core NP02 (Fig. 2d). We note that although westerly strengthening over the NPO is presented in the TraCE-21ka results, as it is in other models<sup>69,71</sup>, we have not taken the higher wind speed into consideration because past studies indicate a lack of correlation between wind speed and dust content in the open ocean<sup>20,58,59</sup>. In terms of the dust deposition process over the NPO, wet deposition is the dominant removal process<sup>23</sup>. Simulated precipitation and moisture anomalies from the TraCE-21ka experiments change little during the H1 event over the studied area (Fig. 4), which excludes it as an additional contributor to core NP02 dust variations.

Our findings also reconcile apparently contrasting interpretations of a previously reported westerly change in China. For proximal dust deposition in China, larger aeolian dust grain size indicates stronger wind intensity due to westerlies shifting closer to dust deposition regions<sup>14</sup>. Based on grain-size analyses, loess records indicate northward-shifted westerlies during H stadials, whereas evidence from Lake Qinghai sediments suggests southward-shifted westerlies<sup>13,14</sup> (Fig. 2e and f). We note that eastern Central Asian loess records (e.g., Yumin Loess) fall under the influence of intensified winds with a strong southerly component during H stadials (Fig. 3a), which would have transported coarser grains. Conversely, Lake Qinghai on the northeastern TP (Fig. 1) was influenced by intensified winds with a strong northerly component during H stadials (Fig. 3a) and, therefore, received more coarse-grained material. When viewed in isolation, these regional wind anomalies might suggest extensive northward or southward displacement of the westerlies belt, respectively, but our results identify them as merely regional AMOC-collapse-related meridional anomalies in the westerly wave train.

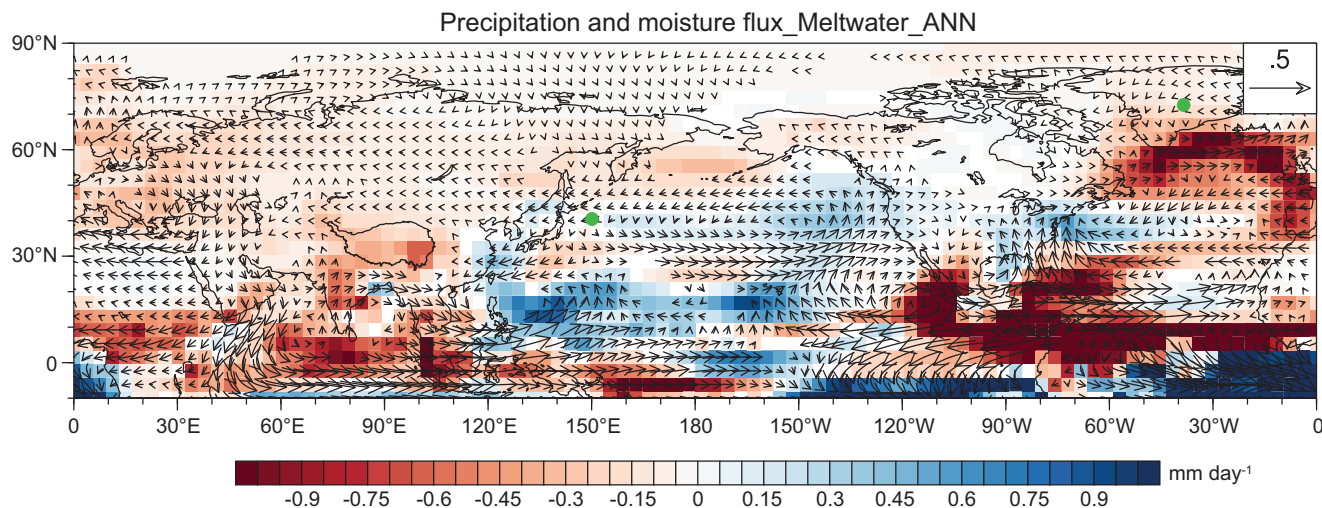


**Fig. 4 Differences in precipitation and moisture flux (black vectors) to water-hosing forcing during H1 in the TraCE-21ka experiment.** Differences are based on model results for freshwater-forcing TraCE-21ka experiments and are denoted as those between two 300-year periods before (19–18.7 ka) and during peak cooling (16–15.7 ka) over the North Atlantic Ocean in H1, respectively. Locations of the Greenland GISP2 ice core and core NPO2 are indicated by green dots.

Finally, we consider distal dust deposition in Greenland, which reveals contrasting temporal variability to that in core NP02 (Fig. 2b and d). In Greenland ice cores, maximum (Asian) dust contents, characterized by higher  $\text{Ca}^{2+}$  concentrations, are found during H stadials, along with lesser peaks during Dansgaard-Oeschger (D-O) stadials<sup>91</sup>. The apparent inconsistency between signals in Greenland ice core and core NP02 can be explained in terms of increased dust transport efficacy to Greenland during D-O stadials. Lower temperatures during cold stadials lead to reduced high northern latitude precipitation<sup>78,92,93</sup>, which reduced wet dust removal from the atmosphere and allowed dust to be transported more efficiently to Greenland. Reduced precipitation en-route has been reproduced for H1 in experiments with both full forcings and meltwater forcings only (Fig. 4), which facilitates dust transport to Greenland. Moreover, both the size distribution of dust in ice cores and circulation models suggest that dust transport times to Greenland were shorter during stadials<sup>94</sup>. Reductions in both transport time and en-route wet deposition increase dust transport efficacy, which in turn is conducive to enhanced dust accumulation in Greenland during D-O stadials. Apart from dust transport efficacy, recent studies suggest that European glacial dust and/or North African dust are potential sources for the last glacial Greenland ice core dust in addition to the Asian interior<sup>95,96</sup>, which may have further increased dust fluxes in Greenland. Our study is more Asian-dust specific and indicates that during H stadials, dust transportation pathways in the Asian dust source region were modified substantially, so that more dust was deposited in the Asian interior, which in turn decreased dust transportation and deposition over the NPO, and impacted the Earth system<sup>83,97</sup>, such as by weakening the NPO iron fertilization effect of phytoplankton productivity.

## Conclusions

Dust plays a crucial role in the Earth system by modulating the global radiation budget and the global carbon cycle<sup>83,97</sup>. NPO dust contents are commonly linked to Asian interior source region climate conditions, with interpretations revolving around extensive poleward westerly shifts during warm states over timescales from a few decades to millions of years<sup>6,98</sup>. However, our reconstructions offer a more nuanced view of changes during abrupt millennial-scale climate events in response to AMOC slowdowns. We find that the westerly dust-transportation

trajectory changed markedly over the Asian interior, setting up a pattern of substantial regional meridional anomalies, while no significant westerly change occurred over the NPO. Our deduced pattern of substantial regional meridional anomalies in westerly circulation over Asia reconciles apparently conflicting results from previous studies that focused on specific regions only. We also reconcile contrasting dust-content changes in Greenland ice cores relative to the NPO, in terms of dust transport efficacy changes between Asia and Greenland with shortened transport times and reduced en-route wet dust deposition during cold stadials.

## Methods

**Laboratory measurements.** Magnetic remanences were measured for cubic samples (8 cm<sup>3</sup>) with a 2-G Enterprises Model 760 R cryogenic magnetometer (sensitivity  $1 \times 10^{-12}$  Am<sup>2</sup>). Isothermal remanent magnetizations (IRMs) were imparted in DC fields of 1 T,  $-0.1$  T, and  $-0.3$  T, which are defined as the saturation IRM (SIRM),  $IRM_{-0.1 T}$ , and  $IRM_{-0.3 T}$ , respectively. The HIRM,  $HIRM_{-0.1 T}$ , and  $L$ -ratio are defined according to refs. 40,46

$$HIRM = (SIRM + IRM_{-0.3 T})/2, \quad (1)$$

$$HIRM_{-0.1 T} = (SIRM + IRM_{-0.1 T})/2 \quad (2)$$

$$L - \text{ratio} = HIRM/[0.5 * (SIRM + IRM_{-0.1 T})], \quad (3)$$

Trace element and rare earth element analyses were made using a Thermo Scientific XSERIES 2 inductively coupled plasma-mass spectrometer (ICP-MS). Samples were freeze-dried and digested with HF-HNO<sub>3</sub> (1:1) in closed Teflon bottles before ICP-MS analysis. Analytical accuracy was assessed with the GSD-9 standard, blank, and replicate measurements.

Clay minerals were identified by X-ray diffraction. Before measurement, samples were treated with 15% H<sub>2</sub>O<sub>2</sub> and then 5% HCl to remove organic matter and carbonate, respectively. Clay-sized particles (<2 μm) were extracted and concentrated with a centrifuge, and were then smeared on glass slides. Analyses were performed with a Rigaku D/max 2500 diffractometer with CuKα radiation at 40 kV voltage and 100 mA current intensity. Peak parameters were estimated semi-quantitatively following ref. 99. Relative contents of smectite, illite, and kaolinite + chlorite were estimated from peak positions at 1.7 nm, 1 nm, and 0.7 nm,

respectively<sup>100</sup>. Relative contents of kaolinite and chlorite were separated according to the relative 0.357 nm and 0.354 nm peak areas.

**Model simulations.** Model data from TraCE-21ka experiments include one full forcing simulation (TraCE-FULL, with transient forcing changes in orbitally driven insolation, atmospheric greenhouse gases, ice sheets, and meltwater fluxes) from 22 ka BP to 1990 CE and four single-forcing simulations (TraCE-ORB, TraCE-GHG, TraCE-ICE, TraCE-MWF), and were employed to evaluate the westerly response to different forcings during past climate changes. For the TraCE-21ka experiments, all simulations were performed using the Community Climate System Model version 3 (CCSM3) from the National Center for Atmospheric Research (NCAR) at T31\_gx3v5 resolution<sup>101</sup>. The atmospheric model is the Community Atmosphere Model 3 with 26 hybrid coordinate levels. The land model includes soil columns, plant types, and land units that specify glaciers, lakes, wetlands, urban areas, and vegetated regions. The ocean model is an implementation of the Parallel Ocean Program in vertical *z*-coordinate with 25 levels. The sea ice model is the NCAR Community Sea Ice Model that includes a subgrid-scale ice thickness distribution. The TraCE-FULL experimental design can be found in Supplementary Fig. 9 and ref.<sup>102</sup>. Each single-forcing experiment was performed with only one evolving forcing with remaining forcings fixed at the same initial conditions as the TraCE-FULL experiment.

TraCE-21ka simulations have been shown to reproduce the H1 and YD events well, which were characterized by a prominent northern hemisphere cooling, especially over the North Atlantic Ocean<sup>103,104</sup>. In this study, two periods of 300 years before and during peak cooling (19–18.7 ka and 16–15.7 ka for H1, 13.2–12.9 ka and 12.3–12 ka for the YD, respectively) were chosen to assess the role of freshwater hosing on westerly climatology differences (Supplementary Note 2).

### Data availability

Data produced in this study are available at Mendeley Data (<https://data.mendeley.com/datasets/42pyc27gy7/2>) via <https://doi.org/10.17632/42pyc27gy7.2>.

### Code availability

The TraCE-21ka code is publicly available at <https://www.cgd.ucar.edu/projects/trace>.

Received: 30 March 2022; Accepted: 1 September 2023;

Published online: 15 September 2023

### References

- Toggweiler, J. R. Shifting westerlies. *Science* **323**, 1434–1435 (2009).
- Montade, V. et al. Teleconnection between the intertropical convergence zone and southern westerly winds throughout the last deglaciation. *Geology* **43**, 735–738 (2015).
- Mölg, T., Maussion, F. & Scherer, D. Mid-latitude westerlies as a driver of glacier variability in monsoonal High Asia. *Nat. Clim. Chang.* **4**, 68–73 (2014).
- Shao, Y. et al. Dust cycle: an emerging core theme in Earth system science. *Aeolian Res.* **2**, 181–204 (2011).
- Zhang, G., Murakami, H., Knutson, T. R., Mizuta, R. & Yoshida, K. Tropical cyclone motion in a changing climate. *Sci. Adv.* **6**, eaaz7610 (2020).
- Yin, J. H. A consistent poleward shift of the storm tracks in simulations of 21st century climate. *Geophys. Res. Lett.* **32**, L18701 (2005).
- Wise, E. K. & Dannenberg, M. P. Reconstructed storm tracks reveal three centuries of changing moisture delivery to North America. *Sci. Adv.* **3**, e1602263 (2017).
- Archer, C. L. & Caldeira, K. Historical trends in the jet streams. *Geophys. Res. Lett.* **35**, L08803 (2008).
- Bond, G. et al. Evidence for massive discharges of icebergs into the North Atlantic Ocean during the last glacial period. *Nature* **360**, 245–249 (1992).
- Broecker, W. S., Peteet, D. M. & Rind, D. Does the ocean-atmosphere system have more than one stable mode of operation? *Nature* **315**, 21–26 (1985).
- Rahmstorf, S. Ocean circulation and climate during the past 120,000 years. *Nature* **419**, 207–241 (2002).
- Hemming, S. R. Heinrich events: massive late Pleistocene detritus layers of the North Atlantic and their global climate imprint. *Rev. Geophys.* **42**, RG1005 (2004).
- Li, Y., Song, Y., Yin, Q., Han, L. & Wang, Y. Orbital and millennial northern mid-latitude westerlies over the last glacial period. *Clim. Dyn.* **53**, 3315–3324 (2019).
- An, Z. et al. Interplay between the westerlies and Asian monsoon recorded in Lake Qinghai sediments since 32 ka. *Sci. Rep.* **2**, 305–307 (2012).
- Nagashima, K. et al. Millennial-scale oscillations of the westerly jet path during the last glacial period. *J. Asian Earth Sci.* **40**, 1214–1220 (2011).
- Seo, I., Lee, Y. I., Yoo, C. M., Kim, H. J. & Hyeong, K. Sr-Nd isotope composition and clay mineral assemblages in eolian dust from the central Philippine Sea over the last 600 kyr: implications for the transport mechanism of Asian dust. *J. Geophys. Res.* **119**, 11492–11504 (2014).
- Li, Y. et al. Westerly jet stream controlled climate change mode since the Last Glacial Maximum in the northern Qinghai-Tibet Plateau. *Earth Planet. Sci. Lett.* **549**, 116529 (2020).
- Tian, F. et al. Environmental variability in the monsoon-westerlies transition zone during the last 1200 years: lake sediment analyses from central Mongolia and supra-regional synthesis. *Quat. Sci. Rev.* **73**, 31–47 (2013).
- Wang, F., Li, Z., Wang, X., Li, B. & Chen, F. Variation and interplay of the Siberian High and westerlies in central-east Asia during the past 1200 kyr. *Aeolian Res.* **33**, 62–81 (2018).
- Rea, D. K. The paleoclimatic record provided by eolian deposition in the deep sea: the geologic history of wind. *Rev. Geophys.* **32**, 159–195 (1994).
- Costa, K. M., McManus, J. F. & Anderson, R. F. Paleoproductivity and stratification across the subarctic Pacific over glacial-interglacial cycles. *Paleoceanogr. Paleoclimatology* **33**, 914–933 (2018).
- Rea, D. K., Leinen, M. & Janecek, T. R. Geologic approach to the long-term history of atmospheric circulation. *Science* **227**, 721–725 (1985).
- Zhao, T. et al. A simulated climatology of Asian dust aerosol and its trans-Pacific transport. Part I: mean climate and validation. *J. Clim.* **19**, 104–122 (2006).
- Maher, B. A. et al. Global connections between aeolian dust, climate and ocean biogeochemistry at the present day and at the last glacial maximum. *Earth-Science Rev.* **99**, 61–97 (2010).
- Kiefer, T., Sarnthein, M., Erlenkeuser, H., Grootes, P. M. & Roberts, A. P. North Pacific response to millennial-scale changes in ocean circulation over the last 60 kyr. *Paleoceanography* **16**, 179–189 (2001).
- Serno, S. et al. Change in dust seasonality as the primary driver for orbital-scale dust storm variability in East Asia. *Geophys. Res. Lett.* **44**, 3796–3805 (2017).
- Hovan, S. A., Rea, D. K., Pisias, N. G. & Shackleton, N. J. A direct link between the China loess and marine  $\delta^{18}\text{O}$  records: aeolian flux to the North Pacific. *Nature* **340**, 296–298 (1989).
- Gai, C. et al. Recording fidelity of relative paleointensity characteristics in the North Pacific Ocean. *J. Geophys. Res. Solid Earth* **126**, e2021JB022068 (2021).
- Inoue, S. & Yamazaki, T. Geomagnetic relative paleointensity chronostratigraphy of sediment cores from the Okhotsk Sea. *Palaeogeogr. Palaeoclimatol. Palaeoecol.* **291**, 253–266 (2010).
- Yamazaki, T., Inoue, S., Shimonoto, T., Sakamoto, T. & Sakai, S. Sea-ice conditions in the Okhotsk Sea during the last 550 kyr deduced from environmental magnetism. *Geochem. Geophys. Geosyst.* **14**, 5026–5040 (2013).
- Lascu, I., Feinberg, J. M., Dorale, J. A., Cheng, H. & Edwards, R. L. Age of the Laschamp excursion determined by U-Th dating of a speleothem geomagnetic record from North America. *Geology* **14**, 139–142 (2016).
- Channell, J. E. T. et al. Magnetic record of deglaciation using FORC-PCA, sortable-silt grain size, and magnetic excursion at 26 ka, from the Rockall Trough (NE Atlantic). *Geochem. Geophys. Geosyst.* **17**, 1823–1841 (2016).
- Lougheed, B. C. & Obrochta, S. P. A rapid, deterministic age-depth modeling routine for geological sequences with inherent depth uncertainty. *Paleoceanogr. Paleoclimatology* **34**, 122–133 (2019).
- Maher, B. A. The magnetic properties of Quaternary aeolian dusts and sediments, and their palaeoclimatic significance. *Aeolian Res.* **3**, 87–144 (2011).
- Dorfman, J. M. et al. A 37,000-year environmental magnetic record of aeolian dust deposition from Burial Lake, Arctic Alaska. *Quat. Sci. Rev.* **128**, 81–97 (2015).
- Larrasoana, J. C., Roberts, A. P., Rohling, E. J., Winkhofer, M. & Wehausen, R. Three million years of monsoon variability over the northern Sahara. *Clim. Dyn.* **21**, 689–698 (2003).



37. Watkins, S. J. & Maher, B. A. Magnetic characterisation of present-day deep-sea sediments and sources in the North Atlantic. *Earth Planet. Sci. Lett.* **214**, 379–394 (2003).
38. Yamazaki, T. & Ioka, N. Environmental rock-magnetism of pelagic clay: implications for Asian eolian input to the North Pacific since the Pliocene. *Paleoceanography* **12**, 111–124 (1997).
39. Zhang, Q. et al. Mechanism for enhanced eolian dust flux recorded in North Pacific Ocean sediments since 4.0 Ma: aridity or humidity at dust source areas in the Asian interior? *Geology* **48**, 77–81 (2020).
40. Robinson, S. G. The late Pleistocene palaeoclimatic record of North Atlantic deep-sea sediments revealed by mineral-magnetic measurements. *Phys. Earth Planet. Inter.* **42**, 22–47 (1986).
41. Bloemendal, J., King, J. W., Hall, F. R. & Doh, S. J. Rock magnetism of late Neogene and Pleistocene deep-sea sediments: relationship to sediment source, diagenetic processes, and sediment lithology. *J. Geophys. Res.* **97**, 4361–4375 (1992).
42. Yamazaki, T. & Ioka, N. Cautionary note on magnetic grain-size estimation using the ratio of ARM to magnetic susceptibility. *Geophys. Res. Lett.* **24**, 751–754 (1997).
43. Itambi, A. C., von Döbenek, T., Mulitza, S., Bickert, T. & Heslop, D. Millennial-scale northwest African droughts related to Heinrich events and Dansgaard-Oeschger cycles: evidence in marine sediments from offshore Senegal. *Paleoceanography* **24**, PA1205 (2009).
44. Ortega-Guerrero, B. et al. Climatic control on magnetic mineralogy during the late MIS 6 - early MIS 3 in Lake Chalco, central Mexico. *Quat. Sci. Rev.* **230**, 106163 (2020).
45. Wells, M. A., Fitzpatrick, R. W., Gilkes, R. J. & Dobson, J. Magnetic properties of metal-substituted haematite. *Geophys. J. Int.* **138**, 571–580 (1999).
46. Liu, Q., Roberts, A. P., Torrent, J., Horng, C. S. & Larrasoana, J. C. What do the HIRM and S-ratio really measure in environmental magnetism? *Geochem. Geophys. Geosyst.* **8**, Q09011 (2007).
47. Jiang, Z., Liu, Q., Barrón, V., Torrent, J. & Yu, Y. Magnetic discrimination between Al-substituted hematites synthesized by hydrothermal and thermal dehydration methods and its geological significance. *J. Geophys. Res. Solid Earth* **117**, B02102 (2012).
48. Ji, J. et al. High resolution hematite/goethite records from Chinese loess sequences for the last glacial-interglacial cycle: rapid climatic response of the East Asian monsoon to the tropical Pacific. *Geophys. Res. Lett.* **31**, L03207 (2004).
49. Rochette, P. et al. Non-saturation of the defect moment of goethite and fine-grained hematite up to 57 Teslas. *Geophys. Res. Lett.* **32**, L22309 (2005).
50. France, D. E. & Oldfield, F. Identifying goethite and hematite from rock magnetic measurements of soils and sediments. *J. Geophys. Res. Solid Earth* **105**, 2781–2795 (2000).
51. Kawai, K., Matsui, H. & Tobo, Y. High potential of Asian dust to act as ice nucleating particles in mixed-phase clouds simulated with a global aerosol-climate model. *J. Geophys. Res. Atmos.* **126**, e2020JD034263 (2021).
52. Lian, S. et al. Global distribution of Asian, Middle Eastern, and North African dust simulated by CESM1/CARMA. *Atmos. Chem. Phys.* **22**, 13659–13676 (2022).
53. Janecek, T. R. & Rea, D. K. Eolian deposition in the northeast Pacific Ocean: Cenozoic history of atmospheric circulation. *Geol. Soc. Am. Bull.* **94**, 730–738 (1983).
54. Janecek, T. R. Eolian sedimentation in the northwest Pacific Ocean: a preliminary examination of the data from Deep Sea Drilling Project Sites 576 and 578. *Initial Rep. Deep Sea Drill. Proj.* **86**, 589–603 (1985).
55. Sun, J., Zhang, M. & Liu, T. Spatial and temporal characteristics of dust storms in China and its surrounding regions, 1960–1999: relations to source area and climate. *J. Geophys. Res. Atmos.* **106**, 10325–10333 (2001).
56. Shen, Z. et al. Characteristics of clay minerals in Asian dust and their environmental significance. *China Particulol.* **3**, 260–264 (2005).
57. Yamazaki, T. Environmental magnetism of Pleistocene sediments in the North Pacific and Ontong-Java Plateau: temporal variations of detrital and biogenic components. *Geochem. Geophys. Geosyst.* **10**, Q07Z04 (2009).
58. Nilson, E. & Lehmküh, F. Interpreting temporal patterns in the late Quaternary dust flux from Asia to the North Pacific. *Quat. Int.* **76–77**, 67–76 (2001).
59. Hovan, S. A., Rea, D. K. & Pisias, N. G. Late Pleistocene continental climate and oceanic variability recorded in northwest Pacific sediments. *Paleoceanography* **6**, 349–370 (1991).
60. Chen, G., Held, I. M. & Robinson, W. A. Sensitivity of the latitude of the surface westerlies to surface friction. *J. Atmos. Sci.* **64**, 2899–2915 (2007).
61. Kidston, J. & Vallis, G. K. The relationship between the speed and the latitude of an eddy-driven jet in a stirred barotropic model. *J. Atmos. Sci.* **69**, 3251–3263 (2012).
62. Vallis, G. K., Zurita-Gotor, P., Cairns, C. & Kidston, J. Response of the large-scale structure of the atmosphere to global warming. *Q. J. R. Meteorol. Soc.* **141**, 1479–1501 (2015).
63. Ait Brahim, Y. et al. North Atlantic ice-rafting, ocean and atmospheric circulation during the Holocene: insights from western Mediterranean speleothems. *Geophys. Res. Lett.* **46**, 7614–7623 (2019).
64. Henry, L. G. et al. North Atlantic ocean circulation and abrupt climate change during the last glaciation. *Science* **353**, 470–474 (2016).
65. Menviel, L. C., Skinner, L. C., Tarasov, L. & Tzedakis, P. C. An ice-climate oscillatory framework for Dansgaard-Oeschger cycles. *Nat. Rev. Earth Environ.* **1**, 677–693 (2020).
66. Ganopolski, A. & Rahmstorf, S. Rapid changes of glacial climate simulated in a coupled climate model. *Nature* **409**, 153–158 (2001).
67. Lynch-Stieglitz, J. The Atlantic meridional overturning circulation and abrupt climate change. *Ann. Rev. Mar. Sci.* **9**, 83–104 (2017).
68. Sun, Y. et al. Influence of Atlantic meridional overturning circulation on the East Asian winter monsoon. *Nat. Geosci.* **5**, 46–49 (2012).
69. Wu, L., Li, C., Yang, C. & Xie, S.-P. Global teleconnections in response to a shutdown of the Atlantic meridional overturning circulation. *J. Clim.* **21**, 3002–3019 (2008).
70. Timmermann, A. et al. The influence of a weakening of the Atlantic meridional overturning circulation on ENSO. *J. Clim.* **20**, 4899–4919 (2007).
71. Okumura, Y. M., Deser, C., Hu, A., Xie, S. P. & Timmermann, A. North Pacific climate response to freshwater forcing in the subarctic North Atlantic: oceanic and atmospheric pathways. *J. Clim.* **22**, 1424–1445 (2009).
72. Zhang, X., Li, J., Gao, M. & Jin, L. Simulated precipitation changes in central Asia since the Last Glacial Maximum. *Quat. Int.* **490**, 82–97 (2018).
73. Thornalley, D. J. R., McCave, I. N. & Elderfield, H. Freshwater input and abrupt deglacial climate change in the North Atlantic. *Paleoceanography* **25**, PA1201 (2010).
74. Carlson, A. E. What caused the Younger Dryas cold event? *Geology* **38**, 383–384 (2010).
75. Álvarez-Solas, J. et al. Heinrich event 1: an example of dynamical ice-sheet reaction to oceanic changes. *Clim. Past* **7**, 1297–1306 (2011).
76. Broecker, W. S. Salinity history of the northern Atlantic during the last deglaciation. *Paleoceanography* **5**, 459–467 (1990).
77. Alley, R. B. Wally was right: predictive ability of the North Atlantic ‘conveyor belt’ hypothesis for abrupt climate change. *Annu. Rev. Earth Planet. Sci.* **35**, 241–272 (2007).
78. Kageyama, M. et al. Climatic impacts of fresh water hosing under last glacial Maximum conditions: a multi-model study. *Clim. Past* **9**, 935–953 (2013).
79. Swingedouw, D. et al. Impact of freshwater release in the North Atlantic under different climate conditions in an OAGCM. *J. Clim.* **22**, 6377–6403 (2009).
80. Manabe, S. & Stouffer, R. J. Two stable equilibria of a coupled ocean-atmosphere model. *J. Clim.* **1**, 841–866 (1988).
81. Schiller, A., Mikolajewicz, U. & Voss, R. The stability of the North Atlantic thermohaline circulation in a coupled ocean-atmosphere general circulation model. *Clim. Dyn.* **13**, 325–347 (1997).
82. Vellinga, M. & Wood, R. A. Global climatic impacts of a collapse of the Atlantic thermohaline circulation. *Clim. Change* **54**, 251–267 (2002).
83. Uno, I. et al. Asian dust transported one full circuit around the globe. *Nat. Geosci.* **2**, 557–560 (2009).
84. Rea, D. K. & Leinen, M. Asian aridity and the zonal westerlies: late Pleistocene and Holocene record of eolian deposition in the northwest Pacific Ocean. *Palaeogeogr. Palaeoclimatol. Palaeoecol.* **66**, 1–8 (1988).
85. Grousset, F. E. et al. Patterns of ice-rafted detritus in the glacial North Atlantic (40–55° N). *Paleoceanography* **8**, 175–192 (1993).
86. Peck, V. L., Hall, I. R., Zahn, R. & Scourse, J. D. Progressive reduction in NE Atlantic intermediate water ventilation prior to Heinrich events: response to NW European ice sheet instabilities? *Geochem. Geophys. Geosyst.* **8**, Q01N10 (2007).
87. Gwiazda, R. H., Hemming, S. R. & Broecker, W. S. Provenance of icebergs during Heinrich event 3 and the contrast to their sources during other Heinrich episodes. *Paleoceanography* **11**, 371–378 (1996).
88. Yu, E.-F., Francois, R. & Bacon, M. P. Similar rates of modern and last-glacial ocean thermohaline circulation inferred from radiochemical data. *Nature* **379**, 689–694 (1996).
89. Henderson, G. M. & Anderson, R. F. The U-series toolbox for paleoceanography. *Rev. Mineral. Geochemistry* **52**, 493–531 (2003).
90. Turney, C. S. M. et al. High-precision dating and correlation of ice, marine and terrestrial sequences spanning Heinrich event 3: testing mechanisms of interhemispheric change using New Zealand ancient kauri (*Agathis australis*). *Quat. Sci. Rev.* **137**, 126–134 (2016).
91. Rohling, E. J., Mayewski, P. A. & Challenor, P. On the timing and mechanism of millennial-scale climate variability during the last glacial cycle. *Clim. Dyn.* **20**, 257–267 (2003).
92. Tegen, I. & Rind, D. Influence of the latitudinal temperature gradient on soil dust concentration and deposition in Greenland. *J. Geophys. Res. Atmos.* **105**, 7199–7212 (2000).
93. Werner, M. et al. Seasonal and interannual variability of the mineral dust cycle under present and glacial climate conditions. *J. Geophys. Res.* **107**, 4744 (2002).



94. Fischer, H., Siggaard-Andersen, M. L., Ruth, U., Röthlisberger, R. & Wolff, E. Glacial/interglacial changes in mineral dust and sea-salt records in polar ice cores: sources, transport, and deposition. *Rev. Geophys.* **45**, RG1002 (2007).
95. Újvári, G. et al. Two possible source regions for central Greenland last glacial dust. *Geophys. Res. Lett.* **42**, 10399–10408 (2015).
96. Újvári, G. et al. Greenland ice core record of Last Glacial dust sources and atmospheric circulation. *J. Geophys. Res. Atmos.* **127**, e2022JD036597 (2022).
97. Schepanski, K. Transport of mineral dust and its impact on climate. *Geosciences* **8**, 151 (2018).
98. Abell, J. T., Winckler, G., Anderson, R. F. & Herbert, T. D. Poleward and weakened westerlies during Pliocene warmth. *Nature* **589**, 70–75 (2021).
99. Biscaye, P. E. Mineralogy and sedimentation of recent deep-sea clay in the Atlantic Ocean and adjacent seas and oceans. *Bull. Geol. Soc. Am.* **76**, 803–832 (1965).
100. Holtzapffel, T. *Les minéraux argileux, préparation, analyse diffractométrique et détermination*. (Société géologique du Nord Publication, 1985).
101. Collins, W. D. et al. The Community Climate System Model version 3 (CCSM3). *J. Clim.* **19**, 2122–2143 (2006).
102. He, F. *Simulating transient climate evolution of the last deglaciation with CCSM3*. PhD Thesis, Univ. Wisconsin-Madison (2011).
103. Shakun, J. D. et al. Global warming preceded by increasing carbon dioxide concentrations during the last deglaciation. *Nature* **484**, 49–54 (2012).
104. Liu, Z. et al. Transient simulation of last deglaciation with a new mechanism for Bølling-Allerød warming. *Science* **325**, 310–314 (2009).
105. Seierstad, I. K. et al. Consistently dated records from the Greenland GRIP, GISP2 and NGRIP ice cores for the past 104 ka reveal regional millennial-scale  $\delta^{18}\text{O}$  gradients with possible Heinrich event imprint. *Quat. Sci. Rev.* **106**, 29–46 (2014).
106. Böhm, E. et al. Strong and deep Atlantic meridional overturning circulation during the last glacial cycle. *Nature* **517**, 73–76 (2015).

## Acknowledgements

We acknowledge the China Ocean Sample Repository for providing samples. We thank the four anonymous reviewers and the Editor Kerstin Schepanski for their valuable comments that improved this study. This study was supported by the National Natural Science Foundation of China (42204080, 92158208, 42261144739, and 42274094), the Australian Research Council (DP200100765), Shenzhen Science and Technology Program (KQTD20170810111725321), the Fund of Laoshan Laboratory (LSKJ202204200), China Postdoctoral Science Foundation (2021M701557). Z. Shi acknowledges support from the Strategic Priority Research Program of Chinese Academy of Sciences (XDB40030000) and the Youth Innovation Promotion Association of the Chinese Academy of Sciences.

## Author contributions

Q.S.L. led the study. C.C.G., A.P.R., D.H., Q.S.L., and Z.G.S. prepared the first draft of the manuscript. C.C.G. developed the NP02 dust record. C.C.G., A.P.R., D.H., and E.J.R. generated the age model. J.W. and Z.G.S. assisted with model simulations. Y.G.L. provided the samples. C.C.G., Y.G.L., J.X.L., and Y.Z. undertook laboratory analyses. All authors discussed and reviewed the paper before submission.

## Competing interests

The authors declare no competing interests.

## Additional information

**Supplementary information** The online version contains supplementary material available at <https://doi.org/10.1038/s43247-023-00987-z>.

**Correspondence** and requests for materials should be addressed to Yanguang Liu or Qingsong Liu.

**Peer review information** *Communications Earth & Environment* thanks Yassine Ait-Brahim, Marlos Goes and the other, anonymous, reviewer(s) for their contribution to the peer review of this work. Primary Handling Editors: Kerstin Schepanski and Joe Aslin.

**Reprints and permission information** is available at <http://www.nature.com/reprints>

**Publisher's note** Springer Nature remains neutral with regard to jurisdictional claims in published maps and institutional affiliations.



**Open Access** This article is licensed under a Creative Commons Attribution 4.0 International License, which permits use, sharing, adaptation, distribution and reproduction in any medium or format, as long as you give appropriate credit to the original author(s) and the source, provide a link to the Creative Commons licence, and indicate if changes were made. The images or other third party material in this article are included in the article's Creative Commons licence, unless indicated otherwise in a credit line to the material. If material is not included in the article's Creative Commons licence and your intended use is not permitted by statutory regulation or exceeds the permitted use, you will need to obtain permission directly from the copyright holder. To view a copy of this licence, visit <http://creativecommons.org/licenses/by/4.0/>.

© The Author(s) 2023